JOURNAL OF GEOPHYSICAL RESEARCH, VOL. 115, A03204, doi:10.1029/2009JA014191, 2010



# Plasma refilling rates for $L$ = 2.3–3.8 flux tubes

Yuki Obana,[1,2] Frederick W. Menk,[1] and Ichiro Yoshikawa[2]

Received 25 February 2009; revised 11 September 2009; accepted 5 October 2009; published 6 March 2010.

[1] Measurements of the eigenfrequency of geomagnetic field lines can provide information on the plasma mass density near the equatorial plane of the magnetosphere. Data from an extended meridional array of ground magnetometers therefore allow the radial density distribution, and its temporal variation, to be remotely monitored. Using cross-phase analysis of magnetometer array data, we determined the equatorial mass density during three moderate geomagnetic storms in March 2004 and June and April 2001. In each case the field line eigenfrequency increased markedly, corresponding to reductions in mass density and indicating that the plasmapause moved earthward and these flux tubes were depleted. We then measured the rate at which these flux tubes were refilled to prestorm levels. This took 2–3 days for $L$ = 2.3 flux tubes, 3 days at $L$ = 2.6, and over 4 days for $L$ > 3.3. Plasmaspheric refilling progressed with a clear diurnal variation associated with linearly increasing plasma density in the daytime and decreasing plasma density at nighttime. The daytime increases in plasma mass density related to refilling rates ranging from ~250 to ~13 amu cm$^{-3}$ h$^{-1}$ over $L$ = 2.3–3.8. The resultant upward plasma flux at the 1000 km level was in the range 0.9–5.2 × 10$^8$ amu cm$^{-2}$ s$^{-1}$. We also determined the daily averaged refilling rate to be ~420 amu cm$^{-3}$ d$^{-1}$ at $L$ = 2.9–3.1, including the nighttime downward flux. By comparison with Imager for Magnetopause-to-Aurora Global Exploration–EUV and VLF whistler data we were able to estimate the plasma composition and found the $O^+$ proportion was of order 3%–7% at $L$ = 2.3 and 6%–13% at $L$ = 3.0.

**Citation:** Obana, Y., F. W. Menk, and I. Yoshikawa (2010), Plasma refilling rates for $L$ = 2.3–3.8 flux tubes, *J. Geophys. Res.*, *115*, A03204, doi:10.1029/2009JA014191.

## 1. Introduction

[2] The plasmasphere is a region of low-energy ("cold," $T_e \sim 1$ eV or less), dense plasma in the inner magnetosphere, comprising mainly electrons and ions that have diffusively migrated from the underlying ionosphere. The behavior of the plasmaspheric plasma population has been previously studied using a variety of techniques. For example, observations of lightning-generated VLF whistlers [e.g., *Park*, 1970] provide information on the radial distribution of electron density in the inner magnetosphere with a time resolution allowing variations to be monitored on hourly scales. However, because of ionospheric absorption, such observations are usually restricted to times when one or both ends of the field lines are in darkness.

[3] Magnetospheric ultralow frequency (ULF) waves that couple to standing field line eigenoscillations (field line resonances (FLRs)) can be used to estimate the plasma mass density near the equatorial plane in the magnetosphere since the resonant frequency depends on the field line length, the magnetic field strength, and the mass density [*Obayashi and Jacobs*, 1958; *Kitamura and Jacobs*, 1968; *Menk et al.*, 1999, and references therein]. In situ spacecraft observations [e.g., *Takahashi and Denton*, 2007] and ground-based measurements [e.g., *Menk et al.*, 2004; *Berube et al.*, 2005] have been used for this purpose. Since the resonances exist almost all the time and at any place (down to $L \sim 1.3$) in the dayside magnetosphere, ground-based observations can provide daytime mass density estimates on hourly time scales. The use of ground magnetometer arrays provides the capability to monitor a wide range of $L$ shells.

[4] Other techniques that have been used to estimate particle densities in the magnetosphere include in situ measurements with particle counters such as electrostatic analyzers [e.g., *Sojka and Wrenn*, 1985], measurements of the path-dependent Doppler shift from satellite-borne beacons [*Poulter et al.*, 1981a, 1981b], and remote sensing using imagers that measure the intensity of resonantly scattered sunlight [e.g., *Sandel and Denton*, 2007]. Coordinated multi-instrument studies have been used to intercalibrate these techniques, determine the radial variation in mass density, and estimate the plasma composition [*Clilverd et al.*, 2003; *Dent et al.*, 2003, 2006; *Grew et al.*, 2007].

[5] These and other techniques can provide information on the location and dynamic behavior of the plasmapause [*Menk et al.*, 2004], the separatrix between particles in the

[1]School of Mathematical and Physical Sciences, University of Newcastle, Newcastle, New South Wales, Australia.
[2]Department of Earth and Planetary Science, University of Tokyo, Tokyo, Japan.


0148-0227/10/2009JA014191$09.00

outer magnetosphere (where motions are dominated by solar wind–driven convection), and the nearly corotating population in the plasmasphere that originates from and is dynamically connected with the underlying ionosphere [e.g., *Carpenter and Park*, 1973]. Properties of the plasmasphere are determined by the pressure balance and hence particle flow along flux tubes linking to the ionosphere, and erosion of the plasmapause boundary under the influence of variable convection processes in the outer magnetosphere. The simplest scenario, in which plasma flows upward from the ionosphere during the daytime, with a corresponding downward flux at night, is greatly modified during and following magnetic storms. During storms the plasmapause is eroded earthward [e.g., *Murakami et al.*, 2007], and sunward directed plumes drain plasmaspheric material into the outer magnetosphere [*Goldstein et al.*, 2004]. Subsequent refilling of depleted plasmaspheric flux tubes normally takes a few days [e.g., *Park*, 1974].

[6] The refilling process has received considerable attention through observational and modeling studies. Here we simply highlight a few representative studies for middle to low latitudes. *Park* [1970] and *Tarcsai* [1985] used whistler observations to determine the electron flux to and from the ionosphere over $L$ = 3.5–5.0 and $L$ = 2.0–2.8, respectively. Park found that under quiet geomagnetic conditions this was $\sim 3 \times 10^8$ el cm$^{-2}$ s$^{-1}$ (referenced to 1000 km altitude) upward on the dayside and $\sim 1.5 \times 10^8$ el cm$^{-2}$ s$^{-1}$ downward on the nightside, while Tarcsai reported that fluxes were usually $< 6 \times 10^8$ el cm$^{-2}$ s$^{-1}$ and mostly downward from 1700–0400 LT. *Saxton and Smith* [1989] also used whistler observations and estimated the daytime upward flux at $L$ = 2.5 was 1–3 $\times 10^8$ el cm$^{-2}$ s$^{-1}$.

[7] *Evans and Holt* [1978] used incoherent scatter measurements to investigate electron density and $H^+$ and $O^+$ fluxes at $L$ = 3.2. They concluded that the upward daytime $H^+$ flux is $\sim 5 \times 10^7$ el cm$^{-2}$ s$^{-1}$ near sunspot maximum and $\sim 10^8$ el cm$^{-2}$ s$^{-1}$ near sunspot minimum. The flux remains upward at night in summer near sunspot maximum but is downward before sunrise at sunspot minimum. Ground-based measurements (via cross-phase analysis) of ULF FLRs have also been used to estimate the upward plasma flux at $L$ = 2 (but mapping to the outer plasmasphere) during the recovery phase of a large storm [*Chi et al.*, 2000]. This was found to be $\sim 6 \times 10^8$ amu cm$^{-2}$ s$^{-1}$.

[8] Sounding measurements from the Radio Plasma Imager (RPI) experiment on the Imager for Magnetopause-to-Aurora Global Exploration (IMAGE) spacecraft can be used to derive the field-aligned electron density profile for a range of $L$ shells [*Reinisch et al.*, 2004]. Focusing on a very large magnetic storm, these authors found that during the main phase flux tubes near local noon were rapidly (<5 h) depleted to <30% of the quiet time content at $L$ = 2.8, while at $L$ = 2.3 there was almost no depletion. They reconciled the region of depletion with inward movement of the plasmapause and hence erosion of the plasmasphere and argued that during refilling the plasmapause does not coincide with the separatrix and in fact may not be sharply defined. They also found that $L$ = 2.5–3.3 flux tubes were refilled to near full values within 28 h, significantly faster than predicted by models.

[9] Models of the refilling process were reviewed by *Lemaire and Gringauz* [1998] and essentially comprise hydrodynamic or semikinetic approaches. Refilling involves plasma interaction through wave-particle effects [e.g., *Schulz and Koons*, 1972], Coulomb collisions [e.g., *Rasmussen and Schunk*, 1988], electrostatic shocks from plasma [e.g., *Banks et al.*, 1971], differences in light and heavy ion behavior [e.g., *Young et al.*, 1979], and the various microscopic and macroscopic plasma processes of ionosphere-magnetosphere coupling.

[10] Using a semikinetic simulation including Coulomb collision effects, *Wilson et al.* [1992] suggested a two-stage refilling process. In the early refilling stage, the upflowing thermal ions coming from the ionosphere must be subsequently pitch angle scattered to become trapped and accumulate in the refilling plasmasphere. When the plasma density becomes high enough, collisions take over the capture and thermalization process. In the late refilling stage, the ion distributions tend to be isotropic, and the temperature decreases with increasing density. The turning point between these two stages depends on the $L$ shell. According to Wilson et al.'s simulation, this occurs for the $L$ = 3 flux tube about 6 h after the initiation of refilling, for $L$ = 4 after about 12 h, for $L$ = 5 after about 19 h, and for $L$ = 6 after about 28 h.

[11] In this paper we investigate the refilling rate and upward plasma flux for the dayside over $L$ shells typical of the plasmasphere. For this purpose we use ULF FLR observations from an extended meridional array of ground magnetometers to provide high time resolution measurements of mass density over a range of $L$ shells. By comparison with VLF whistler and IMAGE-EUV observations we also estimate the plasma composition.

## 2. Data and Analysis

### 2.1. Data Set

[12] We examined the temporal variation in plasma mass density during three geomagnetic storm intervals using ground magnetometer data from three arrays in the European sector and two in the American sector. The European arrays were the Sub-Auroral Magnetometer Network (SAMNET), the British Geological Survey (BGS) array, and the International Monitor for Auroral Geomagnetic Effects (IMAGE), while the American arrays were Magnetometers Along the Eastern Atlantic Seaboard for Undergraduate Research and Education (MEASURE) and the Canadian Magnetic Observatory System (CANMOS). Station locations are described in Table 1.

[13] The first event is from the interval 7–14 March 2004, which includes a moderate geomagnetic storm (minimum $Dst$ = −77 nT) that commenced on 9 March after a magnetically quiet period. The second event is from the interval 17–20 June 2001, when a small geomagnetic storm (minimum $Dst$ = −61 nT) commenced on 18 June. For this interval we have information on the plasmasphere shape via the EUV imager on board the IMAGE spacecraft [*Sandel et al.*, 2001]. The third event we describe is from the interval 24–29 April 2001, during the recovery phase of a moderate geomagnetic storm (minimum $Dst$ = −102 nT) that commenced on 22 April. For this interval we also used EUV images to characterize the plasmapause location and movement.

**Table 1.** Locations of Ground-Based Magnetometer Stations[a]

| Meridian | Station | Code | Geographic Latitude | Geographic Longitude | $L$ Shell ($R_E$) | LT |
|---|---|---|---|---|---|---|
| Scandinavian | Kilpisjarvi | KIL | 69.0°N | 20.8°E | 6.0 | UT + 1 h 23 m |
| | Oulujarvi | OUJ | 64.5°N | 27.2°E | 4.3 | UT + 1 h 49 m |
| | Hankasalmi | HAN | 62.3°N | 26.7°E | 3.7 | UT + 1 h 47 m |
| | Nurmijarvi | NUR | 60.5°N | 24.7°E | 3.4 | UT + 1 h 39 m |
| UK | Faroes | FAR | 62.1°N | 7.0°W | 4.2 | UT − 0 h 28 m |
| | Lerwick | LER | 60.1°N | 1.2°W | 3.6 | UT − 0 h 5 m |
| | Crooktree | CRK | 57.1°N | 2.6°W | 3.0 | UT − 0 h 11 m |
| | Eskdalemuir | ESK | 55.3°N | 3.2°W | 2.7 | UT − 0 h 13 m |
| | York | YOR | 54.0°N | 1.1°W | 2.5 | UT − 0 h 4 m |
| | Hartland | HAD | 51.0°N | 4.5°W | 2.2 | UT − 0 h 18 m |
| American | Ottawa | OTT | 45.4°N | 75.6°W | 3.2 | UT − 5 h 2 m |
| | Clarkson | CLK | 44.7°N | 75.0°W | 3.1 | UT − 5 h 0 m |
| | Millstone Hill | MSH | 42.6°N | 71.5°W | 2.8 | UT − 4 h 46 m |

[a]Shown are the station name, station code, geographic latitude, geographic longitude, $L$ shell (calculated using the IGRF model), and LT of each station relative to UT.

### 2.2. Determination of Mass Density

[14] The procedure for using ground magnetometers to estimate the plasma mass density is to (1) obtain the FLR frequencies from the data, (2) select a suitable magnetic field model, (3) select a suitable description of the variation of plasma mass density along the magnetic field line, and then (4) solve the FLR wave equation for the plasma mass density. We briefly summarize these steps.

#### 2.2.1. Obtain the FLR Frequency

[15] The detection of FLRs from ground magnetometer data is based on the variation in amplitude and phase as a function of frequency and latitude [*Hughes and Southwood*, 1976]. In particular, the "gradient method" [*Baransky et al.*, 1985] and "cross-phase method" [*Waters et al.*, 1991] compare amplitude and phase spectra, in the ULF range, from latitudinally separated ground-based magnetometer pairs to produce an estimate of the local eigenfrequency of the field line whose footpoint lies approximately midway between the two stations. The techniques were previously used by *Menk et al.* [2004], who reported temporal and spatial resolutions of 20–60 min and 0.15–0.4 $R_E$, respectively.

[16] We used these gradient and cross-phase methods in this study. The closely spaced station pairs employed for this analysis are shown in Table 2.

#### 2.2.2. Select a Suitable Magnetic Field Model

[17] As shown in Table 2, midpoints of the station pairs ranged from $L$ = 2.3 to $L$ = 5.0. *Singer et al.* [1981] showed that when using a dipole magnetic field model the daytime fundamental toroidal mode eigenperiod is in error (because of the dipole approximation) by ~10% at 60° geomagnetic latitude, but for $L < 5$ the error is negligibly small under normal conditions. Therefore, we used a dipole model to calculate the field line length and the ambient magnetic field intensity.

#### 2.2.3. Select a Suitable Description of the Variation of Plasma Mass Density Along the Magnetic Field Line

[18] It is often assumed that the field-aligned plasma mass density follows a radial power law dependence of the form

$$\rho(r) = \rho_0 (r_0/r)^m,$$

where $r$ is the geocentric distance along the field line and $r_0$ is the field line distance in the equatorial plane.

[19] The relationship among the frequencies of the harmonics of standing Alfvén waves depends on the variation of plasma mass density along the field line [*Cummings et al.*, 1969]. This in turn means that harmonics of FLR frequencies can be used infer the mass density index: $m$ [*Menk et al.*, 1999; *Takahashi et al.*, 2004]. *Menk et al.* [1999] used harmonics of FLR frequencies to determine $m$ and its diurnal variation. They found $m$ is typically ~3 but shows considerable temporal variation in the range from 1 to 6. *Takahashi et al.* [2004] surveyed 17 months of CRRES data and statistically investigated the harmonic relationship of FLR frequencies. They suggested that $m$ = 0–1 for $L < 6$, corresponding to the plasmasphere.

[20] Recent in situ studies of the field-aligned variation of electron density have found that $m$ = 0–1 in the plasmasphere [*Goldstein et al.*, 2001; *Denton et al.*, 2002a, 2002b], while in

**Table 2.** Station Pairs Used for Cross-Phase Analysis[a]

| Meridian | $\Delta L$ Shell Code | $L$ Shell Midpoint ($R_E$) | L Shell Difference ($R_E$) | LT | $\Delta$LT |
|---|---|---|---|---|---|
| Scandinavian | KIL-OUJ | 5.0 | 1.7 | UT + 1 h 36 m | −0 h 26 m |
| | OUJ-HAN | 4.0 | 0.6 | UT + 1 h 48 m | 0 h 2 m |
| | HAN-NUR | 3.5 | 0.3 | UT + 1 h 43 m | 0 h 8 m |
| UK | FAR-LER | 3.8 | 0.6 | UT − 0 h 16 m | −0 h 23 m |
| | LER-CRK | 3.3 | 0.6 | UT − 0 h 8 m | 0 h 6 m |
| | CRK-ESK | 2.8 | 0.3 | UT − 0 h 12 m | 0 h 2 m |
| | ESK-YOR | 2.6 | 0.2 | UT − 0 h 9 m | −0 h 9 m |
| | YOR-HAD | 2.3 | 0.3 | UT − 0 h 11 m | 0 h 14 m |
| American | OTT-CLK | 3.1 | 0.1 | UT − 5 h 1 m | −0 h 2 m |
| | CLK-MSH | 2.9 | 0.3 | UT − 4 h 53 m | −0 h 14 m |

[a]Shown are the code names of the two stations, $L$ shell of the midpoint between each station pair, difference in $L$ shell between the two stations, local time of the midpoint, and difference in local time between the two stations in each pair.

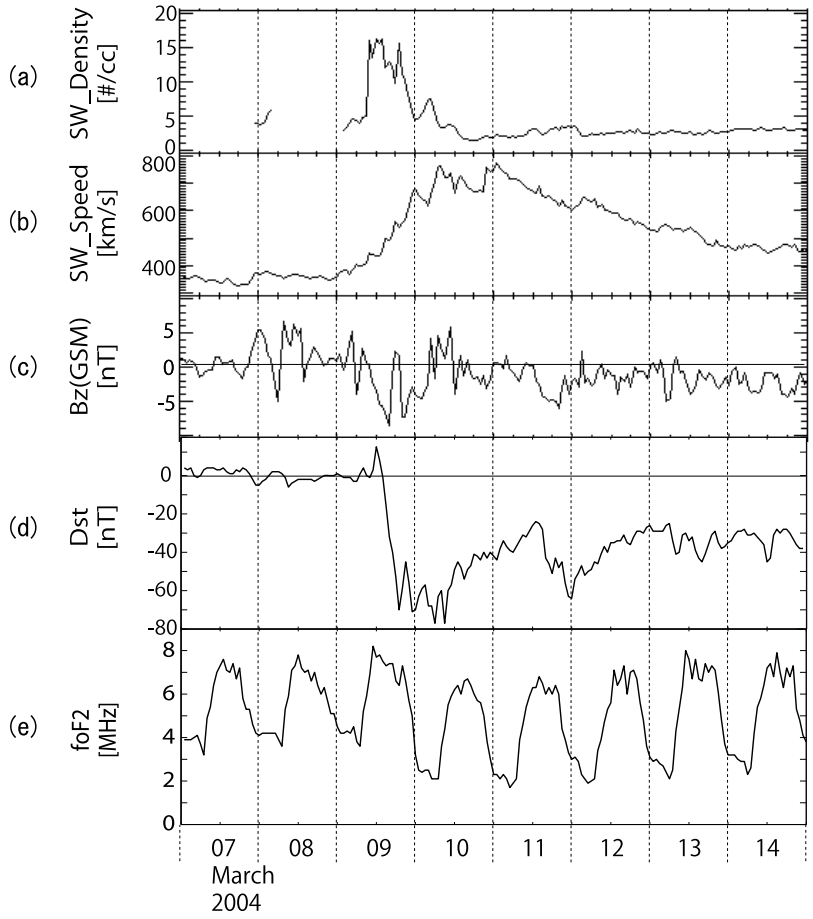


**Figure 1.** General space weather conditions for the interval 7–14 March 2004. (a) Solar wind density, (b) solar wind speed, (c) IMF $B_z$, (d) *Dst* index, and (e) $f_oF_2$ frequency at Chilton. The vertical dashed lines indicate 0000 UT. A recurrent high-speed solar wind stream reached the magnetosphere on 9 March, and an SC was initiated at 1400 UT on 9 March. The *Dst* index reached a minimum value −77 nT at 0900 UT on 10 March.

the plasmatrough larger values of $m$ (from 1.7 to 3) have been found [*Goldstein et al.*, 2001; *Denton et al.*, 2002a, 2002b]. In this study, we have simply used $m = 0$. The exact value of $m$ is not critical [*Menk et al.*, 2004] since the difference in equatorial mass density when choosing $m = 0$ compared to $m = 1$ is only 5% over $L$ = 2.3–4.0.

#### 2.2.4. Solve the FLR Wave Equation for the Plasma Mass Density

[21] We used the approximation describing the relationship between the fundamental toroidal eigenperiod and mass density suggested by *Vellante and Förster* [2006]:

$$T \cong \frac{L^4}{\pi C}\left[4Z_i \int_{-Z_i}^{Z_i} \left(1-z^2\right)^6 \cos^2\left(\frac{\pi}{2}\frac{z}{z_i}\right)\rho(z)dz\right]^{1/2},$$

where $z = \cos(\theta)$ specifies the position along the field line, $z_i$ is the point where the field line meets the ionosphere, $\theta$ is the geomagnetic colatitude, and $C$ is $\sim 1.7 \times 10^4$ if we express density in units of amu cm$^{-3}$ and frequency in mHz. According to Vellante and Förster, this approximation overestimates the actual eigenperiod by only 0.9% and 0.5% for $L$ = 2.66 and $L$ = 1.61, respectively.

[22] In summary, we calculated the equatorial mass density using the above formula with a dipole field and power law index $m = 0$. The anticipated uncertainty is around 15%, arising mostly from uncertainty in measuring the resonance frequency, which typically dominates the errors mentioned above [*Menk et al.*, 2004].

## 3. Event 1: 7–14 March 2004

### 3.1. Variation in Eigenfrequency and Density With *L* Value

[23] Figure 1 shows general space weather information for the interval of interest. The $x$ axis and the vertical dashed lines represent the day of month and 0000 UT on each day, respectively. The parameters plotted are the following: solar wind density, solar wind speed, the $z$ component of interplanetary magnetic field (IMF) $B_z$ (all measured by the ACE spacecraft about 230 $R_E$ upstream), the *Dst* index, and the ionospheric $F$ region critical frequency $f_oF_2$ measured at Chilton in UK (51.70°N, 358.67°E). The 5 days preceding this interval were all geomagnetically quiet, with the daily summed *Kp* (not shown) <13 over 4–5 March and <7 over 6–8 March. A storm was initiated at 1400 UT on

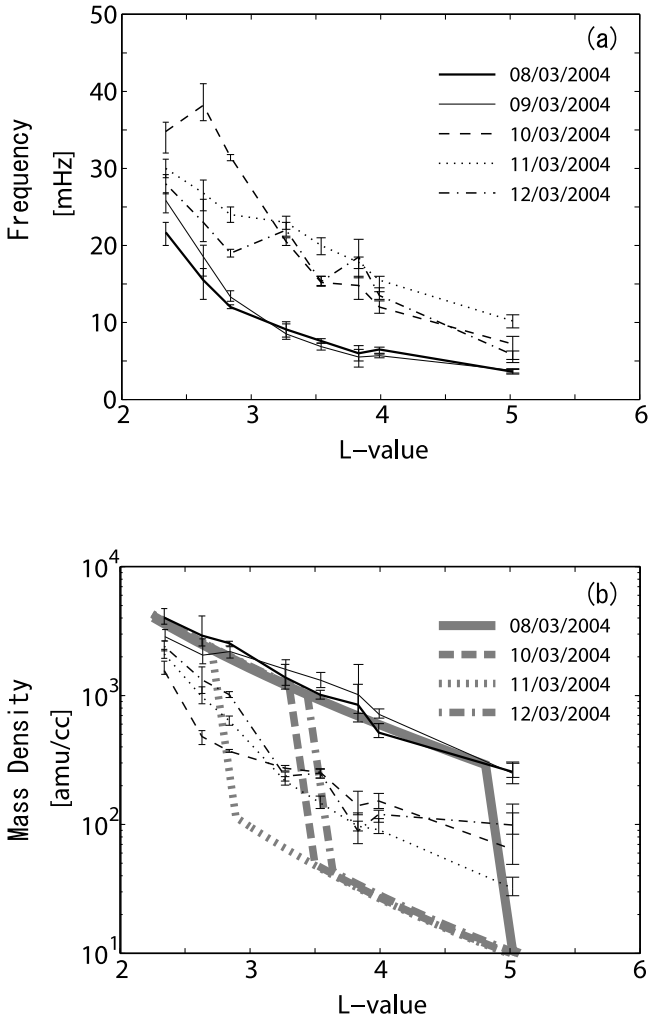


**Figure 2.** $L$ value profile plots for (a) eigenfrequency detected from cross-phase analysis and (b) inferred plasma mass density at the equatorial plane. Solid, dashed, dotted, and dash-dotted lines represent values at 1100 UT on 8, 10, 11, and 12 March 2004, respectively. Thick gray lines in Figure 2b represent the predicted electron mass density at 1100 UT on the above days calculated using the *Carpenter and Anderson* [1992] model.

9 March 2004 by a recurrent high-speed solar wind stream with a maximum speed of 800 km $s^{-1}$. *Dst* reached a minimum of −77 nT at 0900 UT on 10 March. The $f_oF_2$ frequency will be discussed in section 6.7.

[24] Figure 2 shows $L$ shell profiles of eigenfrequencies (Figure 2a) and inferred equatorial plasma mass density (Figure 2b) at 1100 UT on 8 March (thick solid line), 9 March (thin solid line), 10 March (dashed line), 11 March (dotted line), and 12 March (dash-dotted line). All these measurements were from magnetometers in the European sector (~1100 LT and 1230 LT in the UK and Scandinavian meridians, respectively). Error bars represent the uncertainty in determining the exact eigenfrequency from the cross-phase peak and the unity crossing of the interstation power ratio. Thick gray lines in Figure 2b indicate the electron number density profiles for 1100 UT on the above days in the UK meridian determined using the *Carpenter and Anderson* [1992] model.

[25] On 8 and 9 March, one day before and just before the storm commencement, the eigenfrequency was low, and the inferred mass density was high but smoothly decreasing with increasing $L$ value. These features imply flux tubes were saturated because the previous 5 days were quiet. The inferred mass densities show good agreement with the *Carpenter and Anderson* [1992] model electron densities for 8 March for $L < 4.8$. The model predicts that the plasmapause lies at $4.8 < L < 5.0$.

[26] On 10 March, at the beginning of the storm recovery phase, the field line eigenfrequencies were unusually high and inferred mass densities very low for $L > 2.4$, in particular $L = 2.6$. This implies inward erosion of the plasmasphere due to enhanced magnetospheric convection. The model densities suggested that the plasmapause should have been located near $L = 3.4$. On 11 March, mass densities were somewhat higher for $2.4 < L < 3.3$, suggesting that flux tube refilling had commenced. However, beyond $L = 3.3$, the density decreased slightly between 10 and 11 March, suggesting that erosion was continuing in this region. The model suggested that the plasmapause might be located near $L = 3$. By 12 March the mass density had further increased at almost all station pairs except at $L = 3.3$ (LER-CRK) and $L = 3.8$ (FAR-LER). We infer that refilling continued and the plasmapause moved to larger $L$, but perhaps some local structure (e.g., bite-out) was present at $L = 3.3$–3.8 in the UK meridian. We note that the plasmapause is often defined as a sharp density drop as shown in the $L$ shell profiles of the model-predicted electron density. The inferred mass density, however, shows a gentler drop. This may reflect a spatial integration effect of the ionosphere, which smoothes the mass density profiles near the plasmapause [*Poulter and Allan*, 1986; *Menk et al.*, 2004].

### 3.2. Temporal Variation in Mass Density

[27] Figure 3 shows hourly measurements of mass density at $L = 3.8$ (Figure 3a), $L = 3.3$ (Figure 3b), $L = 2.6$ (Figure 3c), and $L = 2.3$ (Figure 3d) over 7–14 March 2004. The error bars again represent the uncertainty in determining an exact eigenfrequency in each case. The vertical shading highlights an interval on 11 March described in more detail in section 3.3.

[28] Over 7–9 March, flux tubes were saturated because of continuing geomagnetically quiet conditions. The average mass density over these three quiet days is shown in Table 3. A storm commenced at 1400 UT on 9 March, and the first data points for the morning of 10 March show low mass densities at all $L$ shells. These flux tubes gradually refilled after 10 March on a time scale that depends on the $L$ shell. At $L = 2.3$, the mass density recovered to its prestorm level in 2 to 3 days and at $L = 2.6$ this took about 3 days. However, at $L = 3.3$ and 3.8, mass densities did not reach prestorm levels after 4 days of refilling (14 March), when a new magnetic disturbance commenced.

### 3.3. Refilling Rate

[29] The shaded section of Figure 3 indicates that mass densities on 11 March increased at a nearly linear rate until 1600 UT. This refilling process is shown in more detail in Figure 4. Crosses indicate hourly measurements of mass

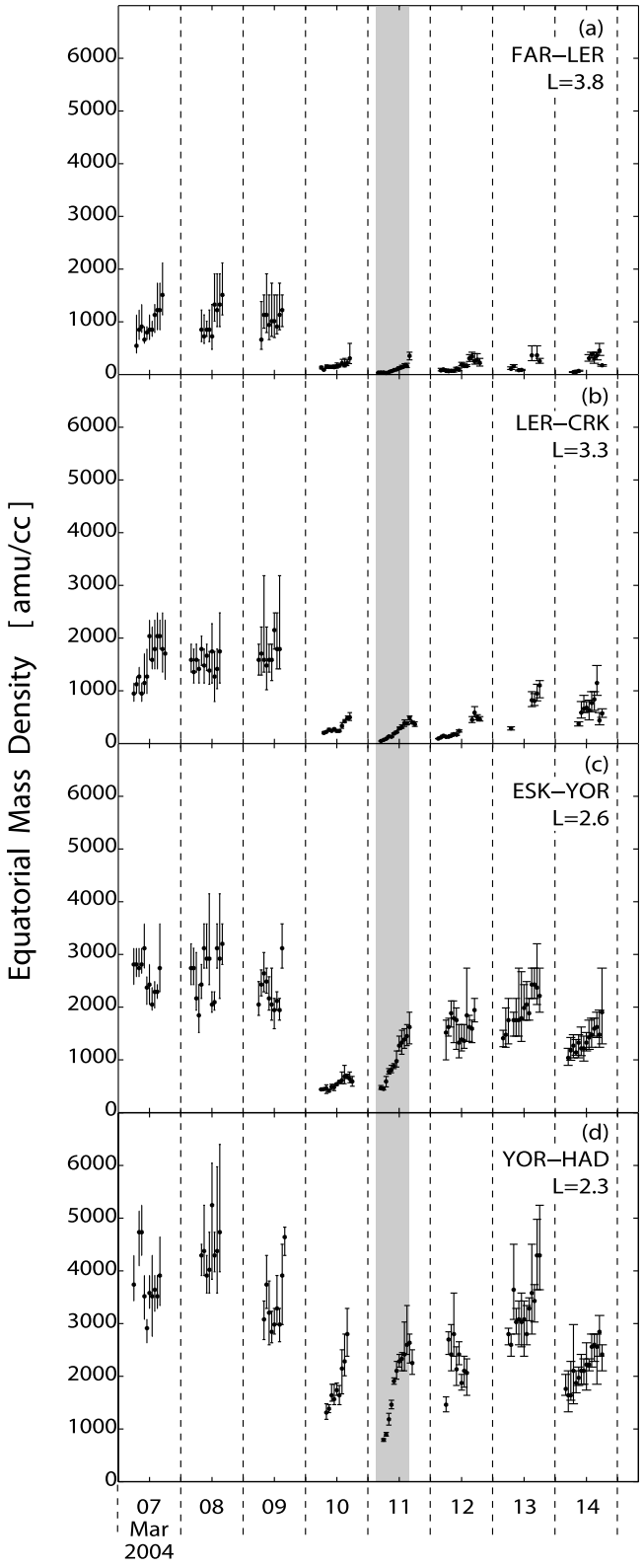


**Figure 3.** Hourly measurements of equatorial plasma mass density at (a) $L$ = 3.8, (b) $L$ = 3.3, (c) $L$ = 2.6, and (d) $L$ = 2.3 over 7–14 March 2004. Vertical shaded interval on 11 March represents an interval examined in detail in Figure 4.

density at $L$ = 3.8 (Figure 4a), $L$ = 3.3 (Figure 4b), $L$ = 2.6 (Figure 4c), and $L$ = 2.3 (Figure 4d). No data are shown after 1600 UT to avoid contamination from a new disturbance. The daytime refilling rate (rate of mass density increase at the equatorial plane) was calculated for each $L$ shell by taking a least squares fit to the linear trend shown. This rate is written in the top right of each plot in units of amu $cm^{-3}$ $h^{-1}$.

[30] The $L$ shell dependence of this refilling rate is depicted by the crosses and solid line in Figure 5a. Error bars indicate the range of standard deviations calculated using the bootstrap method [*Efron*, 1979]. The refilling rate shows a strong $L$ shell dependence: that at $L$ = 2.3 is almost 20 times larger than that at $L$ = 3.8.

[31] A strong $L$ shell dependence of the refilling rate may be attributed to the difference of length and volumes of flux tubes. Refilling is generally believed to arise from the topside ionosphere. While it may be convenient to regard field-aligned flux tubes as having equal cross section at 1000 km altitude, the total tube volume depends on latitude or $L$, as represented schematically in Figure 6. We calculated flux tube volumes in a dipole geometry based on the portion of the tube extending from an area of 1 $cm^2$ at 1000 km altitude to the equatorial plane. We then determined the upward flux of plasma through this area at 1000 km altitude from the rate of change of total mass in these flux tubes.

[32] Figure 5b shows the upward flux of plasma at 1000 km altitude, calculated from the refilling rate shown in Figure 5a. The flux at all $L$ shells was of order $10^8$ amu $cm^{-2}$ $s^{-1}$. The actual values are listed in Table 3. Daytime upward flux observations reported in some previous studies are also shown in Figure 5b. To compare our plasma fluxes with these other measurements, we converted those measurements into plasma mass using a mass loading of 3.0 relative to electron number density [*Park*, 1970; *Saxton and Smith*, 1989] or $H^+$ density [*Evans and Holt*, 1978]. This mass loading number is based on the average ion mass suggested by *Takahashi et al.* [2006]. Our observed plasma fluxes are in good agreement with daytime upward electron and ion fluxes suggested by these previous studies.

[33] It is also evident in Figure 5b that the upward flux at $L$ = 2.3 was 2.6 times larger than that at $L$ = 3.8. We hypothesize that this $L$ shell dependence is related to the solar zenith angle since the Sun is higher in the sky and therefore the ion production rate is higher at lower latitudes compared to higher latitudes. Since the same will happen in the conjugate hemisphere, such an $L$ shell dependence should vary as the average of cosines of solar zenith angles in the Northern and Southern hemispheres. This quantity is represented by the crosses and solid line in Figure 5c. The average value at $L$ = 2.3 is 1.4 times larger than that at $L$ = 3.8. Thus, the solar zenith angle effect is qualitatively consistent with but underestimates the $L$-shell dependence of upward plasma fluxes.

## 4. Event 2: 17–20 June 2001

[34] Figure 7 shows general space weather information for this interval, in the same format as Figure 1, except for $f_oF_2$ data. A storm was initiated early on 18 June because of a

**Table 3.** Mass Density of Saturated Flux Tubes and Upward Ion Flux[a]

| | $L$ = 2.3 | $L$ = 2.6 | $L$ = 2.9 | $L$ = 3.1 | $L$ = 3.3 | $L$ = 3.8 | Units |
|---|---|---|---|---|---|---|---|
| Saturated mass density | 3841 | 2519 | | | 1570 | 1002 | amu cm$^{-3}$ |
| Ion flux | | | | | | | |
| 11 March 2004 | 3.92 | 2.73 | | | 2.25 | 1.38 | $\times 10^8$ (amu cm$^{-2}$ s$^{-1}$) |
| 18 June 2001 | | | 1.71 | 3.46 | | | $\times 10^8$ (amu cm$^{-2}$ s$^{-1}$) |
| 19 June 2001 | | | 3.66 | 5.21 | | | $\times 10^8$ (amu cm$^{-2}$ s$^{-1}$) |
| 25 April 2001 | | | 1.01 | 0.93 | | | $\times 10^8$ (amu cm$^{-2}$ s$^{-1}$) |
| >26 April 2001 | | | 1.20 | 1.16 | | | $\times 10^8$ (amu cm$^{-2}$ s$^{-1}$) |

[a]Shown are the mass density for saturated flux tubes and the upward plasma flux during refilling referenced to 1 cm$^2$ at 1000 km altitude. $L$ values are in $R_E$.

sudden increase in solar wind density simultaneous with an enhancement in the southward component of the IMF. The *Dst* index reached a minimum of −61 nT at 0900 UT. The preceding 4 days had been magnetically quiet. For this interval we consider mass densities deduced using FLR measurements from ground magnetometer pairs in the American meridian with midpoints at $L$ = 3.1 and $L$ = 2.9.

[35] For this interval we can also examine the global shape of the plasmasphere using IMAGE-EUV observations. The EUV imager on board the IMAGE satellite detects EUV light at 30.4 nm, which is resonantly scattered by $He^+$ ions in the plasmasphere. The imager has spatial and temporal resolutions of ~0.1 $R_E$ and ~10 min, respectively, and produces two-dimensional images showing the column density along the line of sight [e.g., *Goldstein et al.*, 2003]. Figure 8a shows four images taken on 18 June 2001 at the times indicated. These are raw images that have not been mapped down to the magnetic equatorial plane. The Earth's apparent size and location are indicated by the black dashed circle in the center of each image. The Sun is to the bottom right in the direction of the white arrows. The light haze around the Earth is the $He^+$ portion of the plasmasphere, glowing at 30.4 nm. Small white circles in each image represent footpoints of field lines from each pair of ground station midpoints mapped to the equatorial plane. Both these midpoints were just outside the plasmapause for each image.

[36] Hourly measurements of mass density at $L$ = 3.1 and $L$ = 2.9 over 17–20 June are shown in Figure 8b. Daytime mass densities dropped suddenly when the storm commenced but then increased almost linearly on 18 June. Vertical arrows indicate the times of the EUV images in

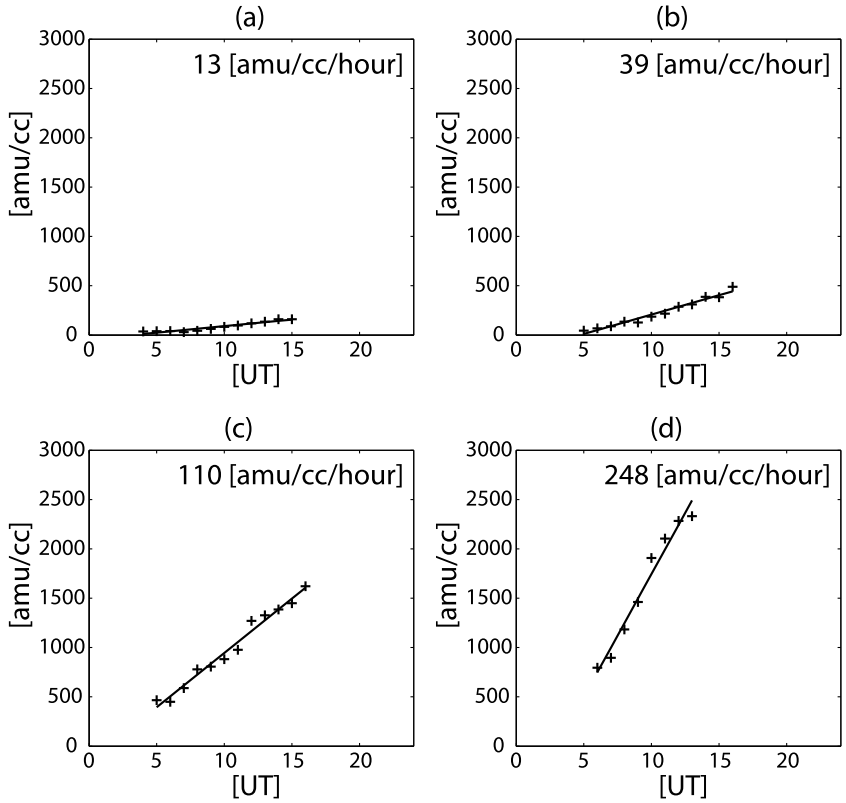


**Figure 4.** Hourly measurements of mass density at (a) $L$ = 3.8, (b) $L$ = 3.3, (c) $L$ = 2.6, and (d) $L$ = 2.3 from 0400 to 1600 UT on 11 March 2004. Numbers in top right of each plot indicate the refilling rate (rate of mass density increase in the equatorial plane) calculated using least squares fitting to the linear functions.

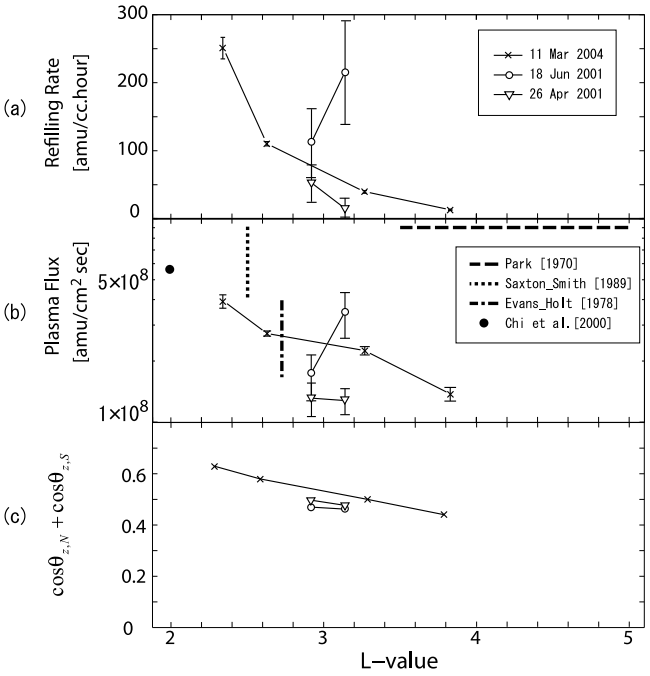


**Figure 5.** $L$ value profiles of (a) the refilling rate at the equatorial plane, (b) the upward flux at 1000 km altitude, and (c) the cosine of the solar zenith angle averaged over the Northern and Southern hemispheres. For Figure 5b the dashed horizontal line, dotted vertical line, dash-dotted vertical line, and solid circles represent the upward flux reported by *Park* [1970], *Saxton and Smith* [1989], *Evans and Holt* [1978], and *Chi et al.* [2000], respectively, converted into plasma mass (amu cm$^{-2}$ s$^{-1}$). See text for further details.

Figure 8a. Densities continued to increase on 19 June before 2000 UT, when another solar wind disturbance occurred.

[37] Using a process similar to that employed above the hourly refilling rates were determined for both $L$ shells on 18 June and are plotted in Figure 5a. These hourly rates are comparable to but slightly larger than on 11 March 2004. Thus on 18 June the flux tubes seem to be refilled effectively even though they map to outside the plasmasphere as defined by a steep $He^+$ density gradient. This result supports *Reinisch et al.*'s [2004] argument that during refilling the plasmapause does not coincide with the separatrix between convecting and corotating plasma flow.

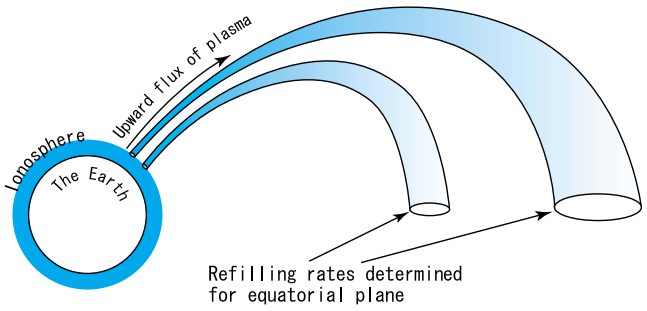


**Figure 6.** Schematic representation of flux tube refilling. We reference the flux to a 1 cm$^2$ cross section at 1000 km altitude, but the volume of each flux tube increases with the $L$ value.

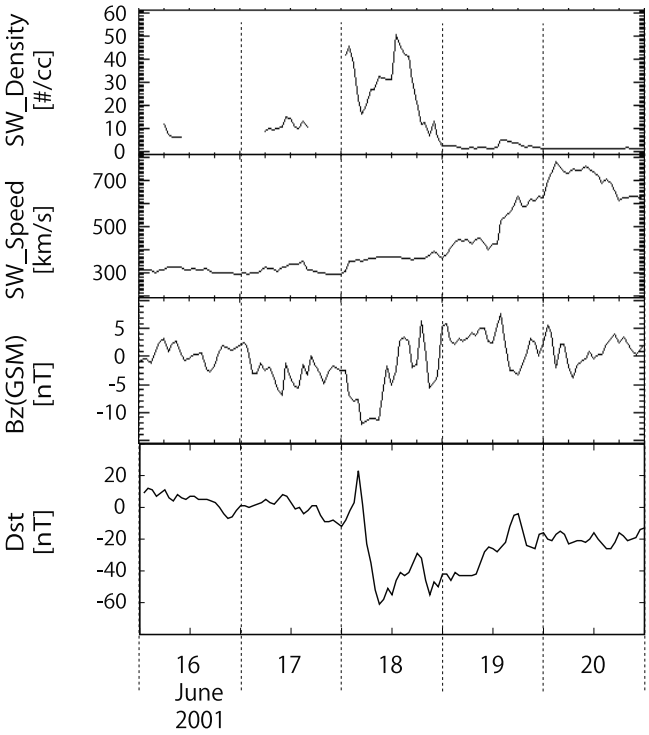


**Figure 7.** General space weather conditions for the interval 16 to 20 June 2001 in the same format as Figure 1, except that $f_oF_2$ data are not included.

[38] The upward fluxes on 18 June, referenced to a cross-sectional area of 1 cm$^2$ at 1000 km, are compared in Figure 5b to the 11 March 2004 values. The fluxes on 18 June are similar to those on 11 March although the $L$ shell dependence shows the opposite trend to the first event. The $L$ shell dependence of the first event probably results from the increase in flux tube volume with the $L$ shell, causing decreasing refilling rates with increasing $L$ shell. For this second event, a different scenario is required, but the explanation is unclear. The actual values are again listed in Table 3. Upward fluxes for 19 June 2001, determined in exactly the same manner as just described for 18 June, are also listed in Table 3. The upward flux increased by a factor of 1.5–2 between 18 and 19 June.

## 5. Event 3: 22–28 April 2001

[39] The third event is from the long recovery phase of a moderate geomagnetic storm that commenced on 21 April (minimum $Dst$ = −102 nT at 1600 UT on that day). Figure 9 shows general space weather information during the interval from 21 to 28 April 2001, in the same format as Figure 7. A storm was initiated late on 21 April because of an enhancement in the southward component of the IMF. The $Dst$ index reached a minimum of −102 nT at 1600 UT on 22 April. Plasma mass density for this interval was deduced using FLR measurements in the American meridian at $L$ = 3.1 and 2.9 in the same manner previously used. Figure 10b shows hourly measurements of mass density over 24–28 April. On 24 April, the mass density could not determine

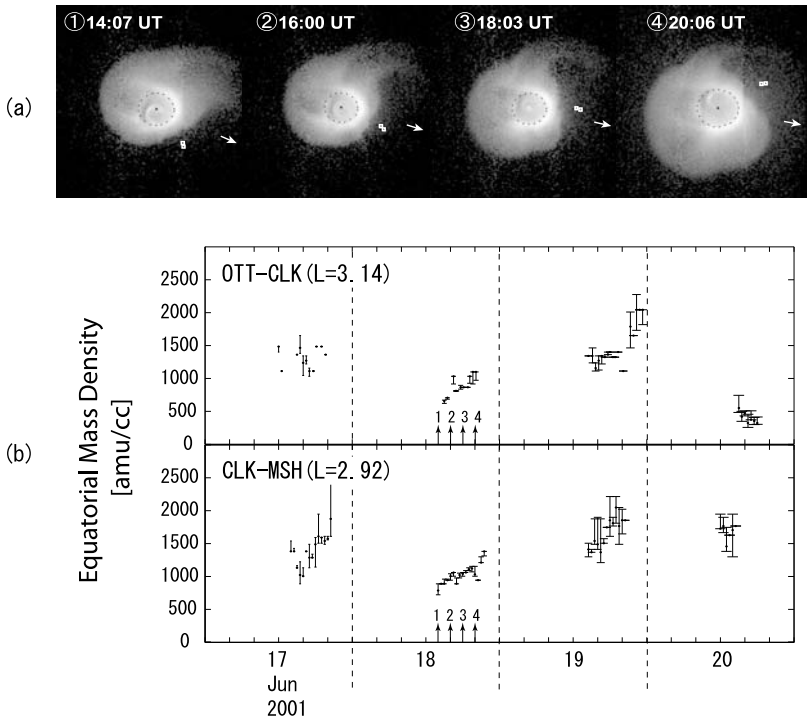


**Figure 8.** (a) Snapshots of the plasmasphere on 18 June 2001 taken by the IMAGE-EUV imager at times indicated. White circles represent footpoints of ground station field lines mapped to the equatorial plane. (b) Hourly measurements of mass density at (top) $L$ = 3.14 and (bottom) $L$ = 2.92 in the American meridian during the interval 17–20 June 2001. Vertical arrows on 18 June show times of EUV images in Figure 8a.

accurately (at $L$ = 2.9) or was very variable ($L$ = 3.1). A linearly increasing trend was evident from 25 to 27 April, and 25 April seems to be the first refilling day.

[40] The hourly refilling rate and upward flux were determined for 25 and 26 April in the same manner previously use and are compared to values for the other events in Figures 5a and 5b and Table 3. The upward fluxes are of the same order of magnitude but smaller than previously but decrease slightly with increasing $L$ value.

[41] IMAGE-EUV observations for this interval are presented in Figure 10a and clearly show that on 25 and 26 April the ground station midpoints mapped to well within the plasmasphere.

## 6. Discussion

### 6.1. Plasmapause Location

[42] Here we consider how the measured upward plasma fluxes relate to the flux tube location within or outside of the plasmasphere. It is tempting to suppose that flux tubes inside the plasmasphere are closed, while those mapping to the outer magnetosphere are subject to convection fields and hence may refill at a different rate.

[43] EUV observations clearly showed that for event 2 (18 June 2001) the $L$= 2.9 and $L$ = 3.1 flux tubes mapped to the equatorial plane outside the plasmasphere, while for event 3 (25 and 26 April 2001) they mapped to inside the plasmasphere.

[44] For event 1, specifically, 11 March 2004 (the day examined in detail), clear EUV images are not available, and four different methods were used to identify the plasmapause location. First, we examined the density-$L$ profile (Figure 2b) for a steep gradient characteristic of the plasmapause. While there is no sharp gradient on 11 March, the

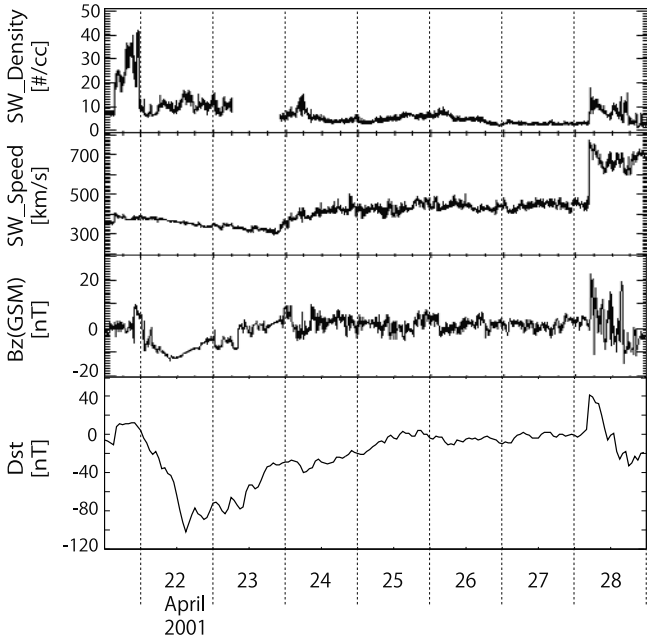


**Figure 9.** General space weather conditions for the interval 21 to 28 April 2001 in the same format as Figure 7.

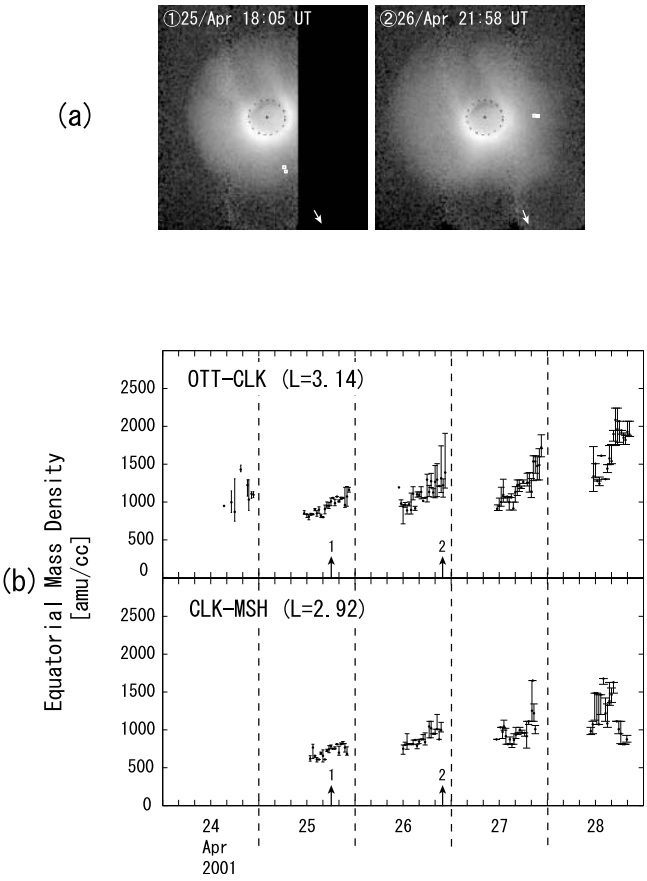


**Figure 10.** (a) Snapshots of the plasmasphere on 25 and 26 April 2001 taken by the IMAGE-EUV imager at times indicated. (b) Hourly measurements of mass density at (top) $L$ = 3.14 and (bottom) $L$ = 2.92 in the American meridian during the interval 24 to 28 April 2001. Format is same as Figure 8.

density dropped significantly between $L$ = 2.8 and $L$ = 3.3. Second, we used *O'Brien and Moldwin*'s [2003] empirical plasmapause location model. The predicted plasmapause location at 1100 UT was in the range $L$ = 2.9–3.2 (depending on whether *Dst* or *Kp* is used as the input parameter). This agrees with the *Carpenter and Anderson* [1992] model prediction shown in Figure 2. Third, we looked for a signature of cross-phase reversal [*Waters*, 2000; *Abe et al.*, 2006; *Kale et al.*, 2007] or disappearance of the cross-phase signature [*Waters*, 2000; *Milling et al.*, 2001], which the above workers have used to identify the plasmapause location. We found a reversal feature for the YOR-HAD ($L$ = 2.2–2.5) pair on 10 March and a disappearance of the phase signature at FAR-LER ($L$ = 3.6–4.2) on 13 and 14 March. Finally, we also examined Defence Meteorological Satellite Program (DMSP)/SSJ particle spectrogram data. On 11 March the 30 eV electron flux profiles showed sharp step-like changes near $L$ = 3.2 at 0800 UT and near $L$ = 3.1 at 1538 UT. From all these, we deduce that at 1100 UT on 11 March the plasmapause (mapped to the European sector) was located near $L$ = 3.

[45] Upward plasma fluxes shown in Figure 5b and Table 3 are similar for all three events, and the presence of the plasmapause near $L$ = 3 on 11 March 2004 does not seem to have affected the flux versus $L$ value profile. There is no evidence in our three case studies that fluxes were greatly different for plasmaspheric flux tubes or flux tubes mapping to just outside the plasmasphere. Upward flow continued from the ionosphere into depleted flux tubes in either case. However, there are a number of signs that suggest the refilling rate is somewhat variable. For event 3, the observed flux tubes mapped to inside the plasmapause and upward plasma fluxes were smaller than those for the other events. This may reflect a lower refilling rate for less completely eroded flux tubes. However, for event 2 the observed flux tubes were mapped to outside of the plasmapause, and upward plasma fluxes were relatively large. This may reflect more vigorous refilling for fully eroded flux tubes. Large upward flux values also imply that plasma provided from the ionosphere is trapped efficiently, i.e., that the flux tubes were probably located inside of the separatrix. This result supports *Reinisch et al.*'s [2004] suggestion that the plasmapause and the separatrix do not coincide during refilling periods.

[46] For event 1, the $L$-shell profile of the upward flux indicates a slightly distorted curve. The points at $L$ = 2.6 or 3.8 seem to be below the trend, or conversely the point at $L$ = 3.3 is above the trend. For $L$ = 2.6, inside of the plasmapause, the refilling rate may be lower for the same reason as for event 3. For $L$ = 3.3, just outside of the plasmapause, refilling may be more vigorous for the same reason as for event 2. Also, for $L$ = 3.8, outside of the plasmapause, a smaller value of upward flux may reflect inefficient trapping of plasma outside of the separatrix. Further observations are required to clarify these matters.

### 6.2. Daily Refilling Rate

[47] Hourly measurements of mass density in this study clearly show that refilling progresses through the upward supply of plasma on the dayside and downward loss of plasma on the nightside. In some previous observational and simulation studies, refilling rates were determined with respect to a day-to-day increase in plasma density and/or a constant 24 h refilling rate. It needs to be clear that any such expression of a refilling rate is actually the daily average of supply and loss processes and should be distinguished from the refilling rate associated purely with the upward flux on the dayside. Here we will describe the daily averaged value as the "daily refilling rate." The previous studies represented in Figure 5b are all purely dayside ones.

[48] Table 4 compares the daily refilling rate estimated from our measurements and previous observations by *Chi*

**Table 4.** Comparison of Daily Refilling Rates From Our Observations With Results Reported by *Chi et al.* [2000] and *Sandel and Denton* [2007][a]

| Source | $L$ Shell | Refilling Rate | Units |
|---|---|---|---|
| Our observations | $L$ = 2.3 | 426 ± 162 | amu cm$^{-3}$ d$^{-1}$ |
| | $L$ = 2.6 | 423 ± 104 | amu cm$^{-3}$ d$^{-1}$ |
| *Chi et al.* [2000] | $L$ = 2 | 647 | amu cm$^{-3}$ d$^{-1}$ |
| Our observations | $L$ = 2.3 | 1.36 ± 0.52 | He$^+$ cm$^{-3}$ h$^{-1}$ |
| | $L$ = 2.6 | 1.35 ± 0.33 | He$^+$ cm$^{-3}$ h$^{-1}$ |
| *Sandel and Denton* [2007] | $L$ = 3.3 | ~1 | He$^+$ cm$^{-3}$ h$^{-1}$ |

[a]Our refilling rates were calculated using plasma mass density observations at 1100 UT on 10, 11, and 12 March 2004 and for comparison purposes were converted to He$^+$ number density by assuming that the H$^+$:He$^+$:O$^+$ proportion was 90:10:0 by number.

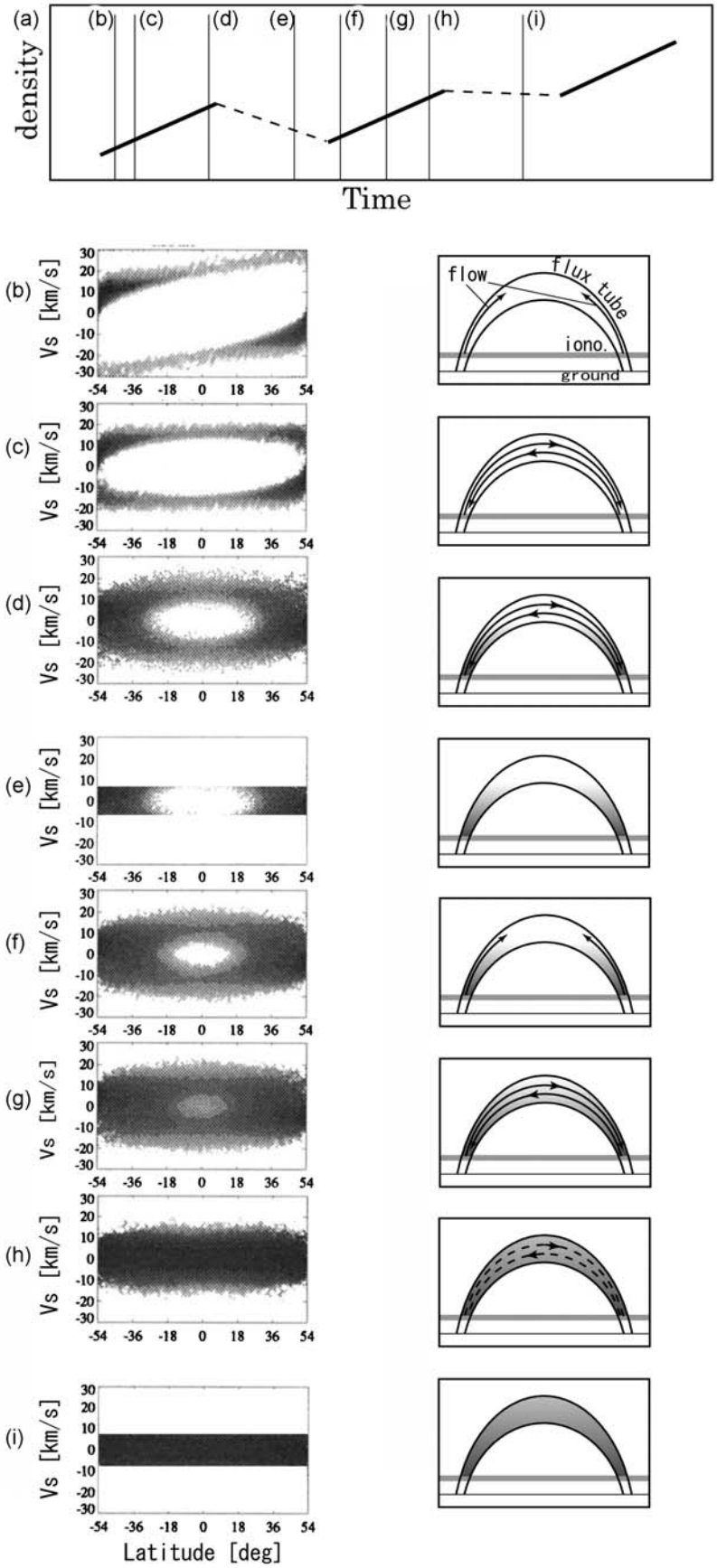
(a)
density
Time
(b)
(c)
(d)
(e)
(f)
(g)
(h)
(i)
Vs [km/s]
Latitude [deg]
flow
flux tube
iono.
ground

**Figure 11**

*et al.* [2000] and *Sandel and Denton* [2007]. Our daily refilling rate was calculated by comparing the change in mass density between 1100 UT on 10 March, 1100 UT on 11 March, and 1100 UT on 12 March 2004. The average and deviation of the difference in mass density between 10–11 March and 11–12 March give the daily refilling rate and its error range as shown in Table 4. This deviation between the two sets of dates may be associated with a two-step refilling process, as described in section 6.8. This procedure was done at $L$ = 2.3 and $L$ = 2.6, and both values are about 420 amu cm$^{-3}$ d$^{-1}$. *Chi et al.*'s [2000] value was also based on cross-phase measurements of plasma mass density.

[49] To compare with *Sandel and Denton*'s [2007] observations, which relate to the daily $He^+$ refilling rate inside the plasmasphere determined using IMAGE-EUV, we converted our observed mass densities into $He^+$ number densities by assuming that the plasma comprised 90% $H^+$ and 10% $He^+$. The resultant $He^+$ refilling rates are also listed in Table 4 and also show reasonable agreement with the previous measurements.

[50] Note that inferring the $He^+$ refilling rate from the cross-phase measurements in this way carries more uncertainty because ion composition can vary over a wide range. *Farrugia et al.* [1989] studied GOES/ICE data and found the ratio of $N^+_{He}/N^+_H$ varies from 0.01 to 0.5 with the most frequent values being between 0.02 and 0.1. The average value of $N^+_{He}/N^+_H$ obtained from the DE-1 mission is about 0.2 [*Newberry et al.*, 1989]. If the ratio of $N^+_{He}/N^+_H$ increases from 0.1 to 0.2, our inferred $He^+$ refilling rate increases by 63%. Furthermore, we have neglected the contribution of heavy ions, in particular $O^+$. Assuming a 1% or 3% fraction of $O^+$ reduces the inferred $He^+$ refilling rate by 10% or 26%, respectively. Nevertheless, our estimate shows reasonable agreement with the measurement of *Sandel and Denton* [2007]. If the $O^+$ density were comparable to the $H^+$ density [e.g., *Horwitz et al.*, 1984], then our inferred $He^+$ refilling rate would be greatly affected [*Fraser et al.*, 2005] and would no longer show such agreement.

[51] It is also worth considering whether the reported refilling rate is inside/outside the plasmapause/separatrix. *Chi et al.* [2000] found very low (~1000 amu cm$^{-3}$) mass density at $L$ = 2 on the first refilling day. The estimated convection electric field supported erosion at $L \sim 2$. At least just after the erosion, the observed flux tube was outside of both plasmapause and separatrix. *Sandel and Denton* [2007] observed inward movement of the plasmapause which reached $L$ = 3–4 during the erosion period. This implies their refilling rate is inside (outside) of the plasmapause at least $L < 3$ ($L > 4$).

### 6.3. Diurnal Refilling Process

[52] Figure 3 shows that storm time mass density and hence refilling exhibits a strong diurnal trend, with particle loss from flux tubes in the nightside. However, there are differences from one day and night to another (e.g., between the evening and morning of 10–11 March compared to the evening and morning of 11–12 March) that may be due to other effects.

[53] The refilling process may take place as illustrated schematically in Figure 11. Figure 11a represents a mass density time series for the first 3 days of refilling. Solid and dashed diagonal lines represent day and night side densities, respectively, and vertical lines labeled b–i indicate times corresponding to Figures 11b–11i. Figures 11b–11i (left) are adapted from *Wilson et al.* [1992, Figure 5] and represent phase space plots for $H^+$ ions in an $L$ = 4 flux tube. Wilson et al.'s model of refilling is based on a kinetic description of the plasma with the effect of Coulomb collisions. The horizontal and vertical axes show position (latitude along the field line) and velocity along the field line, respectively. Figures 11b–11i (right) illustrate the refilling process at each time. The black and gray horizontal lines denote the ground and ionosphere, and curved lines represent the flux tube. Arrows and gray shading within the flux tube indicate plasma flow and trapped plasma, respectively.

[54] At the beginning of refilling as shown in Figures 11b (left) and 11b (right), the initial ion beams flow out from the ionosphere. Two counterstreaming beams are established along the full length of the flux tube (Figures 11c (left) and 11c (right)) and gradually merge together (Figures 11d (left) and 11d (right)). During the first night this upward plasma flow diminishes or ceases and particles having finite velocity reenter and are lost to the ionosphere (Figures 11e (left) and 11e (right)). Refilling recommences the next morning. The two counterstreaming beams reform and merge via collisional processes (Figures 11f–11h). During the second night particles having finite velocities are again lost to the ionosphere but to a lesser extent because of the progress of trapping (Figures 11i (left) and 11i (right)). Therefore, the loss rate is different between the first and second nights of refilling.

[55] There is a further, geographical effect. We assume that the rate of daytime ion production in the ionosphere, and hence the upward flux, depends at least in part on the solar zenith angle. However, this angle varies with season and latitude. *Obana et al.* [2008] showed that there is a strong asymmetry in conjugate ionospheric Pedersen conductances for field lines where one footpoint is in darkness while the other is in daylight. This effect arises from the difference between geomagnetic and geographic coordinates and is most pronounced at American longitudes [*Clilverd et al.*, 2007].

[56] Figure 5c shows the solar zenith angle for European sector magnetometer stations in March. It is interesting to compare the averaged solar zenith angle effect cos ($\theta_N$) + cos ($\theta_S$) for the UK sector and American sector stations shown in Table 2, for the three events studied here. The times considered are 1200 UT for event 1 and 1700 UT

**Figure 11.** (a) Schematic time series of mass density during the first 3 days of refilling. Solid and dotted lines indicate mass density on the dayside and nightsides, respectively. Thin vertical lines labeled (b)–(i) indicate times that correspond to Figures 11b–11i. (b–i) (left) Phase space plots for $H^+$ ions in an $L$ = 4 flux tube [after *Wilson et al.*, 1992, Figure 5]. Horizontal and vertical axes show position (latitude along the field line) and velocity along the field line, respectively. (right) Schematic depictions of the refilling process. Upward arrows arise from the ionospheres, and gray hatching in each flux tube indicates plasma flow and trapped plasma, respectively.

**Table 5.** Nighttime Loss Rates[a]

| Date | $L$ = 2.3 | $L$ = 2.6 | $L$ = 3.3 | $L$ = 3.8 | Units |
|---|---|---|---|---|---|
| *Based on Density Decrease During the Night-Day Gap in FLR Data* | | | | | |
| 9 Mar 2004 | 208 (4.5) | 178 (5.7) | 93 (4.3) | 73 (6.0) | amu cm$^{-3}$ h$^{-1}$ |
| 10 Mar 2004 | 143 (5.1) | 11 (1.6) | 37 (7.5) | 25 (8.2) | amu cm$^{-3}$ h$^{-1}$ |
| 11 Mar 2004 | 60 (2.3) | 7 (0.4) | 36 (7.4) | 23 (6.5) | amu cm$^{-3}$ h$^{-1}$ |
| 12 Mar 2004 | - | 48 (2.5) | 21 (3.9) | 10 (3.0) | amu cm$^{-3}$ h$^{-1}$ |
| *Based on Short Intervals of FLR Data at Night* | | | | | |
| 10 Mar 2004 | - | 48 (7.0) | - | - | amu cm$^{-3}$ h$^{-1}$ |
| 11 Mar 2004 | - | - | 64 (13.1) | - | amu cm$^{-3}$ h$^{-1}$ |
| 12 Mar 2004 | - | - | 63 (10.8) | 40 (11.8) | amu cm$^{-3}$ h$^{-1}$ |

[a]Determined from the decrease in mass density during the day-night gap in FLR data and from short intervals at local night when FLR signatures were observed. $L$ values are in $R_E$.

for events 2 and 3, corresponding to local noon in the UK and American sectors. As shown in Figure 5c, the averaged solar zenith angles are similar for all three events, although the contributions from the Northern and Southern hemispheres are quite different. In the American sector, there is a large difference in geographic latitude between the magnetic conjugate points because of the difference between the geomagnetic and geographic coordinate systems. For example, the geographic latitudes of the midpoint of the OTT-CLK pair and its conjugate point are 45°N and 70°S, respectively.

[57] In June at 1700 UT (~1200 LT at OTT-CLK, ~1100 LT at its conjugate point) the Southern Hemisphere footpoints for $L$ = 2.9–3.1 American sector flux tubes are in darkness, but the Sun is almost overhead in the Northern Hemisphere. In April, this asymmetry is reduced but is still evident. In the European sector, the difference in geographic latitude between conjugate points is relatively small. For example, the latitude of the midpoint of the LER-CRK pair and its conjugate point is 58°N and 55°S. In March at 1200 UT (~1200 LT at LER-CRK and ~1400 LT at its conjugate point) the solar zenith angle is almost the same at both ends of the UK flux tube. In summary, the contribution from the Northern Hemisphere at noon is approximately 50%, 100%, and 90% for events 1, 2, and 3, respectively (not shown). Therefore, although the total upward flux is the same in each case, there is a strong asymmetry in the contributions from each ionosphere.

### 6.4. $L$ Shell Dependence of Upward Plasma Flux

[58] As described in sections 3.3 and 6.3, we assumed that the rate of ion production in the daytime ionosphere and hence the upward plasma flux depends at least in part on the solar zenith angle.

[59] As shown in Figure 5c, the averaged zenith angle for all three events decreased with increasing $L$ shell. This is obvious because the sun rises higher at lower latitudes. As shown in Figure 5b, the upward flux for events 1 and 3 also decreased with increasing $L$ shell. This trend supports the above mentioned assumption, but the solar zenith angle effect alone is insufficient to explain the extent to which flux varies with $L$.

[60] However, the upward flux for event 2 shows an opposite $L$ shell trend, and other unknown factors seem to play a role. We speculate that the fact that this is the only event in which the flux tubes were clearly confirmed to be outside of the plasmasphere may play a role. For example, as discussed in section 6.2, an $L$ shell variation in the composition of the upward plasma flux may have a significant effect. We also note that the difference in solar zenith angle between the Northern and the Southern hemispheres was largest for this event. Finally, variations in the trapping mechanisms in the magnetosphere and ionospheric transport processes may play a role. These are issues for future investigation.

### 6.5. Downward Plasma Flux

[61] In this study we monitored the storm time mass density through FLR measurements, but FLRs do not show clear cross-phase signatures at nighttime, and therefore we cannot normally observe the nighttime decrease in mass density in our data. However, this is possible occasionally for short intervals in the evening sector (e.g., in Figure 3 at $L$ = 2.6 on 10 March, $L$ = 3.3 on 11 and 12 March, and $L$ = 3.8 on 12 March). We have used the density decrease during these short intervals to estimate the downward plasma flux during those times. We also estimated the downward flux from the decrease in density occurring over the night-to-day gaps in the FLR data.

[62] The resultant loss rates are shown in Table 5. Data for loss rate calculated from the night-to-day gaps refer to the night between that evening and the next morning; for example, 9 Mar 2004 refers to the night of 9–10 March. Numbers in parentheses indicate the loss rate normalized to the maximum observed density prior to nighttime. Because many factors can affect the loss of cross-phase signature and the downward flux, these values should be regarded as first-order estimates only. In particular, loss rates estimated from the night-day gap are widely scattered. We can speculate about two possible reasons for this. The first concerns the length of time for which FLR data are unobtainable, which ranged from 9 to 14 h. This variable gap length may cause an apparent difference in amount of plasma loss in the nightside. The second possibility is an actual change in the loss rate of plasma.

[63] Nevertheless, the average nighttime loss rate seems to be around 50–60 amu cm$^{-3}$ h$^{-1}$. It is unclear whether this depends on $L$ shell. Normalized loss rates show a more coherent distribution. The average normalized loss rates calculated using the gap and the short time methods are 4.6 ± 2.3 and 10.7 ± 2.6 [$\times 10^2$], respectively, where the error range indicates the standard deviation. The maximum density in the preceding daytime appears to influence the loss rate in the subsequent nighttime. For example, hourly loss rate seems to be restricted to ~10% of the maximum density prior to the nighttime.

### 6.6. Ion Composition

[64] In order to estimate the ion composition, we have compared FLR mass density estimates to electron density information deduced from whistler observations based on VLF Doppler shift measurements at Rothera, Antarctica. The technique was described by *Clilverd et al.* [2003]. At $L$ = 2.3 at 1300 UT (0900 LT) on 11 March 2004 we found the electron density to be 720 cm$^{-3}$. The plasma mass density deduced from FLR measurements at 0900 LT at YORHAD ($L$ = 2.3) was 1461 amu cm$^{-3}$. The ion mass loading factor was thus 2.03 (note, however, that there is a 4 h LT difference between the VLF and cross-phase measurements which could affect these results). Since we have no informa-

tion on the $He^+$ concentration we then calculated the ion composition for four cases: $He^+$ abundance ratio = 0%, 5%, 10%, and 20%. The ion composition by the number of $H^+$:$He^+$:$O^+$ for these four situations was 93:0:7, 89:5:6, 85:10:5, and 77:20:3, respectively. Therefore, the $O^+$ proportion was in the range 3%–7%. This is low compared to what is expected for an $O^+$ torus [*Fraser et al.*, 2005].

[65] The availability of IMAGE-EUV data, in particular, for 1800–2000 UT on 18 June (event 2) allows us to estimate the composition of the upward plasma flux. The EUV camera consists of three identical sensor heads [*Sandel et al.*, 2001]. During the interval examined, the footpoints of the observed field lines were within the field of view of only one of these sensor heads, so we can avoid dispersion of the estimated $He^+$ density due to the uncertainty of intercalibration between the sensor heads. The estimation was achieved in the following way. First, we scaled the EUV observations at the equatorial footpoints of the observed field lines at $L$ = 2.9 and 3.1 for 1800, 1900, and 2000 UT on 18 June to obtain an estimate of the $He^+$ column abundance in $cm^{-2}$, $N$, as described by *Gallagher et al.* [2005, Appendix A]. This was then used to determine the $He^+$ number density $\rho = N/l$, where $l$ is the integration length. Next, we assumed that the average ion mass is 2.03 or 3.0 amu, as suggested by the above mentioned estimation for event 1 and by *Takahashi et al.* [2006], respectively. When compared to the FLR-derived mass density, this allows the total ion number density to be obtained. The ion composition by the number of $H^+$:$He^+$:$O^+$ for $L$ = 2.9–3.1 was thus found to be 92:2:6 and 84:3:13 for the two cases in which the ion mass was assumed to be 2.03 and 3.0 amu, respectively. Although just estimates, these numbers suggest a somewhat rich heavy ion component.

### 6.7. Negative Ionospheric Storm

[66] The ionosphere is the source of plasmaspheric plasma. It is therefore interesting to consider how the state of the ionosphere during magnetic storms affects or is affected by flux tube refilling and depletion processes. For this purpose we studied the $F_2$ layer critical frequency $f_oF_2$ using this as a proxy for ionization changes in the $F$ layer. Figure 1e shows $f_oF_2$ measurements from the UK sector for event 1, in which a negative ionospheric storm (decrease in $f_oF_2$ compared to typical daily values) can clearly be seen during the recovery phase of the geomagnetic storm. It is tempting to suppose that the ionospheric density was diminished because of its supplying plasma into the eroded plasmasphere.

[67] Negative ionospheric storms develop after the onset of a geomagnetic storm during the previous night and are caused by changes in the neutral gas composition [*Prölss*, 1993]. Specifically, the ratio of molecular gas concentration ($N_2$ + $O_2$) to the atomic oxygen concentration is increased mainly through heating at auroral latitudes, leading to a region of increased mean mass that is moved to middle latitudes by the nightside equatorward winds and brought to the dayside as the Earth rotates. Daytime positive storm effects may be due to short duration uplifting of the $F_2$ layer.

[68] Therefore, although it is tempting to speculate that the decrease in $f_oF_2$ is solely due to a local upward flow of electrons and ions, such an interpretation is simplistic and ignores the effect of neutral winds on ionospheric composition and temperature.

### 6.8. Two-Step Refilling

[69] Some studies have suggested that the refilling process has two stages: a supersonic early stage and followed by a subsonic late stage [e.g., *Banks et al.*, 1971]. Observational studies [e.g., *Lawrence et al.*, 1999] and modeling studies [e.g., *Wilson et al.*, 1992] have suggested that the refilling rate in the early stage is smaller than that in the late stage. To which stage(s) do our refilling rate results shown in Figure 5 and Table 3 correspond?

[70] *Lawrence et al.* [1999] studied cold ion density at geosynchronous orbit and showed that the refilling rate is ~0.6–12 $cm^{-3}$ $d^{-1}$ and 10–50 $cm^{-3}$ $d^{-1}$ for the early and later stages, respectively, and the early stage finishes in less than 24 h. The lifetime of this early stage depends on the $L$ value, being shorter at smaller $L$ [*Wilson et al.*, 1992]. Our refilling rates were calculated for $2 < L < 4$ from the mass density on the first and second refilling days. At least the second refilling days (11 March 2004 and 19 June and 26 April 2001) would therefore correspond to the later second stage. We note from Table 3 that the values for April and June 2001 do show an increase in the refilling rate from the first day to the second. The typical increase in rate was 2 and 1.2 for 18–19 June and 25–26 April, respectively. These values seem to be smaller than Lawrence et al's increase in rate, although Lawrence et al.'s observations were widely scattered. On the other hand, *Wilson et al.*'s [1992] simulation for $L$ = 4 showed a smaller increase in upward flux: ~$4.5 \times 10^{-7}$ $cm^{-2}$ $s^{-1}$ at the early time (4 h after refilling commencement) and ~$6 \times 10^{-7}$ $cm^{-2}$ $s^{-1}$ at the later time (16 h after refilling commencement). Our typical increasing rate shows a reasonable agreement with their increasing rate ~1.3, although the duration of the early stage is rather short in Wilson et al.'s result.

### 6.9. Total Time Required to Refill the Flux Tubes

[71] As shown in Figure 3, total time required to refill the flux tube to prestorm level varies with $L$ shell and was estimated to be 2–3 days at $L$ = 2.3, 3 days at $L$ = 2.6, and over 4 days for $L > 3.3$. This result shows reasonable agreement with *Park*'s [1974] whistler observations. He suggested ~1 day at $L$ = 2.5 and ~8 days at $L$ = 4. Using IMAGE-RPI observations, *Reinisch et al.* [2004] found much shorter refilling times: less than 28 h for $L$ = 2.2–3.7. This may be caused by an ambiguity of the start time of refilling or an apparent difference due to the diurnal refilling process and limit of time resolution of observations. These are issues for future investigation.

## 7. Conclusions

[72] Using cross-phase analysis of magnetometer array data from the European and American sectors, we determined the equatorial mass density and its rate of change during three moderate geomagnetic storms in March 2004, June 2001, and April 2001.

[73] The time taken to refill depleted flux tubes was estimated for the event in March 2004 and depends on the $L$ value, and is 2–3 days at $L$ = 2.3, 3 days at $L$ = 2.6, and more than 4 days for $L > 3.3$. This is in good agreement

with *Park*'s [1974] observations but longer than reported by *Reinisch et al.* [2004]. Plasma refilling rates were calculated from the hourly variation of plasma mass density for all of the three storm events. These ranged from ~250 amu cm$^{-3}$ h$^{-1}$ at $L$ = 2.3 to ~13 amu cm$^{-3}$ h$^{-1}$ at $L$ = 3.8. The resultant upward plasma flux at the 1000 km level was 0.9–5.2 × 10$^8$ amu cm$^{-2}$ s$^{-1}$. These values are in reasonable agreement with daytime upward ion and electron fluxes determined by previous authors. The refilling rates for the events in April and June 2001 at $L$ = 2.9 and 3.1 increased from the first refilling day to the second. The rate of increase was 1.2–2, in good agreement with the increasing rate shown in *Wilson et al.*'s [1992] simulation that suggested a two-step refilling process.

[74] Plasmaspheric refilling progresses with a clear diurnal variation associated with supply of plasma from the ionosphere on the dayside and downward loss of plasma on the nightside. The nighttime loss rates were roughly estimated from the night-to-day gaps in FLR data or from short intervals of nighttime FLR data when the mass density was seen to decrease. The loss rates were in the range of 7–208 amu cm$^3$ h$^{-1}$ with a typical value of 50 amu cm$^3$ h$^{-1}$.

[75] We found that the daily averaged refilling rate at $L$ = 2.3 and $L$ = 2.6 was about 420 amu cm$^{-3}$ d$^{-1}$, and this agrees reasonably well with previous measurements [*Chi et al.*, 2000; *Sandel and Denton*, 2007].

[76] By comparing cross-phase, whistler, and IMAGE-EUV observations, we were able to estimate the ion composition of the upward flowing plasma and found that the daytime $O^+$ proportion was in the range of 3%–7% on 11 March 2004 at $L$ = 2.3 and ~6%–13% on 18 June 2001 at $L$ = 2.9–3.1. These values suggest a somewhat rich heavy ion component during these refilling periods.

[77] **Acknowledgments.** We thank the SAMNET, BGS, IMAGE, MEASURE, and CANMOS teams for magnetometer data. SAMNET is operated by the Department of Communications Systems at Lancaster University (U. K.) and has been funded by the Science and Technology Facilities Council (STFC). Data from the IMAGE stations were provided courtesy of the Finnish Meteorological Institute, the University of Oulu, and the Geological Survey of Sweden. The data from BGS stations were provided courtesy of the British Geological Survey. MEASURE is operated by IGPP, University of California, Los Angeles, and the Florida Institute of Technology, Melbourne, Florida. CNMOS is operated by the Geological Survey of Canada, part of Natural Resources Canada. We thank B. R. Sandel (University of Arizona) for IMAGE-EUV data and M. Clilverd (British Antarctic Survey) for Rothera VLF data. We thank the ACE spacecraft, ACE MAG instrument, and ACE SWEPAM instrument teams and N. Ness and D. J. McComas for the ACE MAG and SWEPAM data provided through the CDA Web site, respectively. We also thank the groups of SPIDR and WDC for Geomagnetism, Kyoto, for providing $f_oF_2$ data and final *Dst* index, respectively. Finally, we thank the DMSP team for providing DMSP/SSJ data.

[78] Zuyin Pu thanks Zoe Kale and another reviewer for their assistance in evaluating this paper.

## References

Abe, S., H. Kawano, J. Goldstein, S. Ohtani, S. I. Solovyev, D. G. Baishev, and K. Yumoto (2006), Simultaneous identification of a plasmaspheric plume by a ground magnetometer pair and IMAGE extreme ultraviolet imager, *J. Geophys. Res.*, *111*, A11202, doi:10.1029/2006JA011653.

Banks, P. M., A. F. Nagy, and W. I. Axford (1971), Dynamical behavior of thermal protons in mid-latitude ionosphere and magnetosphere, *Planet. Space Sci.*, *19*(9), 1053–1067.

Baransky, L. N., Y. E. Borovkov, M. B. Gokhberg, and S. M. Krylov (1985), The gradient-method of measuring the resonance frequencies of magnetic-field lines, *Izv. Akad. Nauk SSSR Ser. Fiz.*, *8*, 74–91.

Berube, D., M. B. Moldwin, S. F. Fung, and J. L. Green (2005), A plasmaspheric mass density model and constraints on its heavy ion concentration, *J. Geophys. Res.*, *110*, A04212, doi:10.1029/2004JA010684.

Carpenter, D. L., and R. R. Anderson (1992), An ISEE/whistler model of equatorial electron-density in the magnetosphere, *J. Geophys. Res.*, *97* (A2), 1097–1108.

Carpenter, D. L., and C. G. Park (1973), On what ionospheric workers should know about the plasmapause-plasmasphere, *Rev. Geophys. Space Phys.*, *11*(1), 133–154.

Chi, P. J., C. T. Russell, S. Musman, W. K. Peterson, G. Le, V. Angelopoulos, G. D. Reeves, M. B. Moldwin, and F. K. Chun (2000), Plasmaspheric depletion and refilling associated with the September 25, 1998 magnetic storm observed by ground magnetometers at $L$ = 2, *Geophys. Res. Lett.*, *27*(5), 633–636.

Clilverd, M. A., et al. (2003), In situ and ground-based intercalibration measurements of plasma density at $L$ = 2.5, *J. Geophys. Res.*, *108* (A10), 1365, doi:10.1029/2003JA009866.

Clilverd, M. A., N. P. Meredith, R. B. Horne, S. A. Glauert, R. R. Anderson, N. R. Thomson, F. W. Menk, and B. R. Sandel (2007), Longitudinal and seasonal variations in plasmaspheric electron density: Implications for electron precipitation, *J. Geophys. Res.*, *112*, A11210, doi:10.1029/2007JA012416.

Cummings, W., R. O'Sullivan, and P. Coleman Jr. (1969), Standing Alfvén waves in the magnetosphere, *J. Geophys. Res.*, *74*(3), 778–793, doi:10.1029/JA074i003p00778.

Dent, Z. C., I. R. Mann, F. W. Menk, J. Goldstein, C. R. Wilford, M. A. Clilverd, and L. G. Ozeke (2003), A coordinated ground-based and IMAGE satellite study of quiet-time plasmaspheric density profiles, *Geophys. Res. Lett.*, *30*(12), 1600, doi:10.1029/2003GL016946.

Dent, Z. C., I. R. Mann, J. Goldstein, F. W. Menk, and L. G. Ozeke (2006), Plasmaspheric depletion, refilling, and plasmapause dynamics: A coordinated ground-based and IMAGE satellite study, *J. Geophys. Res.*, *111*, A03205, doi:10.1029/2005JA011046.

Denton, R. E., J. Goldstein, and J. D. Menietti (2002a), Field line dependence of magnetospheric electron density, *Geophys. Res. Lett.*, *29*(24), 2205, doi:10.1029/2002GL015963.

Denton, R. E., J. Goldstein, J. D. Menietti, and S. L. Young (2002b), Magnetospheric electron density model inferred from Polar plasma wave data, *J. Geophys. Res.*, *107*(A11), 1386, doi:10.1029/2001JA009136.

Efron, B. (1979), Bootstrap methods: Another look at the jackknife, *Ann. Stat.*, *7*(1), 1–26.

Evans, J. V., and J. M. Holt (1978), Nighttime proton fluxes at Millstone Hill, *Planet. Space Sci.*, *26*(8), 727–744.

Farrugia, C. J., D. T. Young, J. Geiss, and H. Balsiger (1989), The composition, temperature, and density structure of cold ions in the quiet terrestrial plasmasphere: GEOS 1 results, *J. Geophys. Res.*, *94*(A9), 11,865–11,891.

Fraser, B. J., J. L. Horwitz, J. A. Slavin, Z. C. Dent, and I. R. Mann (2005), Heavy ion mass loading of the geomagnetic field near the plasmapause and ULF wave implications, *Geophys. Res. Lett.*, *32*, L04102, doi:10.1029/2004GL021315.

Gallagher, D. L., M. L. Adrian, and M. W. Liemohn (2005), Origin and evolution of deep plasmaspheric notches, *J. Geophys. Res.*, *110*, A09201, doi:10.1029/2004JA010906.

Goldstein, J., R. E. Denton, M. K. Hudson, E. G. Miftakhova, S. L. Young, J. D. Menietti, and D. L. Gallagher (2001), Latitudinal density dependence of magnetic field lines inferred from Polar plasma wave data, *J. Geophys. Res.*, *106*(A4), 6195–6201.

Goldstein, J., M. Spasojevi, P. H. Reiff, B. R. Sandel, W. T. Forrester, D. L. Gallagher, and B. W. Reinisch (2003), Identifying the plasmapause in IMAGE EUV data using IMAGE RPI in situ steep density gradients, *J. Geophys. Res.*, *108*(A4), 1147, doi:10.1029/2002JA009475.

Goldstein, J., B. R. Sandel, M. F. Thomson, M. Spasojevic, and P. H. Reiff (2004), Simultaneous remote sensing and in situ observations of plasmaspheric drainage plumes, *J. Geophys. Res.*, *109*, A03202, doi:10.1029/2003JA010281.

Grew, R. S., F. W. Menk, M. A. Clilverd, and B. R. Sandel (2007), Mass and electron densities in the inner magnetosphere during a prolonged disturbed interval, *Geophys. Res. Lett.*, *34*, L02108, doi:10.1029/2006GL028254.

Horwitz, J. L., R. H. Comfort, and C. R. Chappell (1984), Thermal ion composition measurements of the formation of the new outer plasmasphere and double plasmapause during storm recovery phase, *Geophys. Res. Lett.*, *11*(8), 701–704, doi:10.1029/GL011i008p00701.

Hughes, W. J., and D. J. Southwood (1976), The screening of micropulsation signals by the atmosphere and ionosphere, *J. Geophys. Res.*, *81*, 3234–3240.

Kale, Z. C., I. R. Mann, C. L. Waters, J. Goldstein, F. W. Menk, and L. G. Ozeke (2007), Ground magnetometer observation of a cross-phase rever-

sal at a steep plasmapause, *J. Geophys. Res.*, *112*, A10222, doi:10.1029/2007JA012367.
Kitamura, T., and J. A. Jacobs (1968), Determination of the magnetospheric plasma density by the use of long-period geomagnetic micropulsations, *J. Geomagn. Geoelectr.*, *20*, 33–44.
Lawrence, D. J., M. F. Thomsen, J. E. Borovsky, and D. J. McComas (1999), Measurements of early and late time plasmasphere refilling as observed from geosynchronous orbit, *J. Geophys. Res.*, *104*(A7), 14,691–14,704.
Lemaire, J. F., and K. I. Gringauz (1998), *The Earth's Plasmasphere*, Cambridge Univ. Press, Cambridge, U. K.
Menk, F. W., D. Orr, M. A. Clilverd, A. J. Smith, C. L. Waters, D. K. Milling, and B. J. Fraser (1999), Monitoring spatial and temporal variations in the dayside plasmasphere using geomagnetic field line resonances, *J. Geophys. Res.*, *104*(A9), 19,955–19,969.
Menk, F. W., I. R. Mann, A. J. Smith, C. L. Waters, M. A. Clilverd, and D. K. Milling (2004), Monitoring the plasmapause using geomagnetic field line resonances, *J. Geophys. Res.*, *109*, A04216, doi:10.1029/2003JA010097.
Milling, D. K., I. R. Mann, and F. W. Menk (2001), Diagnosing the plasmapause with a network of closely spaced ground-based magnetometers, *Geophys. Res. Lett.*, *28*(1), 115–118.
Murakami, G., M. Hirai, and I. Yoshikawa (2007), The plasmapause response to the southward turning of the IMF derived from sequential EUV images, *J. Geophys. Res.*, *112*, A06217, doi:10.1029/2006JA012174.
Newberry, I. T., R. H. Comfort, P. G. Richards, and C. R. Chappell (1989), Thermal $He^+$ in the plasmasphere: Comparison of observations with numerical-calculations, *J. Geophys. Res.*, *94*(A11), 15,265–15,276.
Obana, Y., F. W. Menk, M. D. Sciffer, and C. L. Waters (2008), Quarter-wave modes of standing Alfvén waves detected by cross-phase analysis, *J. Geophys. Res.*, *113*, A08203, doi:10.1029/2007JA012917.
Obayashi, T., and J. A. Jacobs (1958), Geomagnetic pulsations and the Earth's outer atmosphere, *Geophys. J. R. Astron. Soc.*, *1*(1), 53–63.
O'Brien, T. P., and M. B. Moldwin (2003), Empirical plasmapause models from magnetic indices, *Geophys. Res. Lett.*, *30*(4), 1152, doi:10.1029/2002GL016007.
Park, C. G. (1970), Whistler observation of the interchange of ionization between the ionosphere and the protonosphere, *J. Geophys. Res.*, *75*(22), 4249–4260.
Park, C. G. (1974), Some features of plasma distribution in plasmasphere deduced from antarctic whistlers, *J. Geophys. Res.*, *79*(1), 169–173.
Poulter, E. M., and W. Allan (1986), The ground magnetic-fields of transient ULF pulsations at the plasmapause, *Planet. Space Sci.*, *34*(11), 1073–1079.
Poulter, E. M., J. K. Hargreaves, G. J. Bailey, and R. J. Moffett (1981a), A modeling study of satellite beacon measurements of protonospheric replenishment, *Planet. Space Sci.*, *29*(12), 1281–1286.
Poulter, E. M., J. K. Hargreaves, G. J. Bailey, and R. J. Moffett (1981b), Satellite beacon measurements of protonospheric fluxes, *Planet. Space Sci.*, *29*(12), 1273–1280.
Prölss, G. W. (1993), On explaining the local time variation of ionospheric storm effects, *Ann. Geophys.*, *11*, 1–9.
Rasmussen, C. E., and R. W. Schunk (1988), Multistream hydrodynamic modeling of interhemispheric plasma flow, *J. Geophys. Res.*, *93*(A12), 14,557–14,565.
Reinisch, B. W., X. Huang, P. Song, J. L. Green, S. F. Fung, V. M. Vasyliunas, D. L. Gallagher, and B. R. Sandel (2004), Plasmaspheric mass loss and refilling as a result of a magnetic storm, *J. Geophys. Res.*, *109*, A01202, doi:10.1029/2003JA009948.
Sandel, B. R., and M. H. Denton (2007), Global view of refilling of the plasmasphere, *Geophys. Res. Lett.*, *34*, L17102, doi:10.1029/2007GL030669.
Sandel, B. R., R. A. King, W. T. Forrester, D. L. Gallagher, A. L. Broadfoot, and C. C. Curtis (2001), Initial results from the IMAGE extreme ultraviolet imager, *Geophys. Res. Lett.*, *28*(8), 1439–1442.
Saxton, J. M., and A. J. Smith (1989), Quiet time plasmaspheric electric-fields and plasmasphere ionosphere coupling fluxes at $L$ = 2.5, *Planet. Space Sci.*, *37*(3), 283–293.
Schulz, M., and H. C. Koons (1972), Thermalization of colliding ion streams beyond plasmapause, *J. Geophys. Res.*, *77*(1), 248–254.
Singer, H. J., D. J. Southwood, R. J. Walker, and M. G. Kivelson (1981), Alfven wave resonances in a realistic magnetospheric magnetic field geometry, *J. Geophys. Res.*, *86*(A6), 4589–4596.
Sojka, J. J., and G. L. Wrenn (1985), Refilling of geosynchronous flux tubes as observed at the equator by GEOS 2, *J. Geophys. Res.*, *90*(A7), 6379–6385.
Takahashi, K., and R. E. Denton (2007), Magnetospheric seismology using multiharmonic toroidal waves observed at geosynchronous orbit, *J. Geophys. Res.*, *112*, A05204, doi:10.1029/2006JA011709.
Takahashi, K., R. E. Denton, R. R. Anderson, and W. J. Hughes (2004), Frequencies of standing Alfven wave harmonics and their implication for plasma mass distribution along geomagnetic field lines: Statistical analysis of CRRES data, *J. Geophys. Res.*, *109*, A08202, doi:10.1029/2003JA010345.
Takahashi, K., R. E. Denton, R. R. Anderson, and W. J. Hughes (2006), Mass density inferred from toroidal wave frequencies and its comparison to electron density, *J. Geophys. Res.*, *111*, A01201, doi:10.1029/2005JA011286.
Tarcsai, G. (1985), Ionosphere-plasmasphere electron fluxes at middle latitudes obtained from whistlers, *Adv. Space Res.*, *5*(4), 155–158.
Vellante, M., and M. Förster (2006), Inference of the magnetospheric plasma mass density from field line resonances: A test using a plasmasphere model, *J. Geophys. Res.*, *111*, A11204, doi:10.1029/2005JA011588.
Waters, C. L. (2000), ULF resonance structure in the magnetosphere, in *Coordinated Measurements of Magnetospheric Processes*, *Adv. Space Res.*, *25*(7–8), 1541–1558.
Waters, C. L., F. W. Menk, B. J. Fraser, and P. M. Ostwald (1991), Phase structure of low-latitude Pc3-4 pulsations, *Planet. Space Sci.*, *39*(4), 569–582.
Wilson, G. R., J. L. Horwitz, and J. Lin (1992), A semikinetic model for early stage plasmasphere refilling: 1. Effects of coulomb collisions, *J. Geophys. Res.*, *97*(A2), 1109–1119.
Young, E. R., D. G. Torr, and P. G. Richards (1979), Counterstreaming of $O^+$ and $H^+$ ions in the plasmasphere, *Geophys. Res. Lett.*, *6*(12), 925–928.

F. W. Menk, School of Mathematical and Physical Sciences, University of Newcastle, Newcastle, NSW 2308, Australia.
Y. Obana and I. Yoshikawa, Department of Earth and Planetary Science, University of Tokyo, Tokyo 113-0033, Japan. (obana@eps.s.u-tokyo.ac.jp)